Transverse-spin dependence of the p-p total cross section $\Delta\sigma_T$ from 0.8 to 2.5 GeV/c

W. P. Madigan,* D. A. Bell,† J. A. Buchanan, M. M. Calkin,‡ J. M. Clement, M. Copel, M. D. Corcoran, K. A. Johns, J. D. Lesikar,§ H. E. Miettinen, G. S. Mutchler, C. J. Naudet, G. P. Pepin,** G. C. Phillips, J. B. Roberts, and S. E. Turpin††
T. W. Bonner Nuclear Laboratories, Rice University, Houston, Texas 77251

E. V. Hungerford, B. W. Mayes, A. D. Hancock,‡‡ L. S. Pinsky, and K. K. Sekharan
Physics Department, University of Houston, Houston, Texas 77004

C. L. Hollas and P. J. Riley
Physics Department, University of Texas at Austin, Austin, Texas 78712

J. C. Allred and B. E. Bonner
Los Alamos National Laboratory, Los Alamos, New Mexico 87545

P. Cameron and S. T. Linn§§
Physics Department, University of Michigan, Ann Arbor, Michigan 48104

W. von Witsch
Institut für Strahlen und Kernphysik, Universität Bonn, Bonn, Federal Republic of Germany

M. Furić
Department of Physics, University of Zagreb, Zagreb, Yugoslavia

V. Valković
Institut "Ruder Bosković," Zagreb, Yugoslavia
(Received 15 October 1984)

The difference $\Delta\sigma_T=\sigma(\downarrow\uparrow)-\sigma(\uparrow\uparrow)$ between the proton-proton total cross sections for protons in pure transverse-spin states, was measured at incident momenta 0.8 to 2.5 GeV/c in experiments performed at the Los Alamos Clinton P. Anderson Meson Physics Facility and the Argonne Zero Gradient Synchrotron. In agreement with other data, peaks were observed at center-of-mass energies of 2.14 and 2.43 GeV/c^2, where $^1D_2$ and $^1G_4$ dibaryon resonances have been proposed.

I. INTRODUCTION

The difference $\Delta\sigma_T=\sigma(\downarrow\uparrow)-\sigma(\uparrow\uparrow)$ between the proton-proton total cross sections for antiparallel and parallel initial transverse-spin states is conveniently expressed in terms of an s-channel helicity amplitude at zero scattering angle,

$$\Delta\sigma_T=\frac{4\pi}{k}\mathrm{Im}\phi_2(t=0)\ ,$$

where k is the center-of-mass wave number of one of the protons in the initial state and ϕ_2 is the double-flip, no-net-flip s-channel helicity amplitude.[1,2] The first measurements of $\Delta\sigma_T$ in the early 1970s in the 2-to-10-GeV/c region[3,4] could not be explained by Regge-exchange theory.[5,6] Subsequent measurements of $\Delta\sigma_T$, including the present experiment, and the corresponding longitudinal quantity $\Delta\sigma_L$ revealed rich structure in the 0.8-to-2.5-GeV/c region.[7–9] This surprising new structure has stimulated a great deal of theoretical activity.[10–19] Phase-shift analyses indicating resonancelike structure in several partial waves $^1D_2$, $^3F_3$, and $^1G_4$ at masses of 2.14, 2.22, and 2.43 GeV/c^2, respectively, led some researchers to propose the existence of dibaryon resonances at those masses.[12,13,20] The widths of the proposed resonances are 0.05–0.10 GeV (2.14 GeV/c^2), 0.10–0.20 GeV (2.22 GeV/c^2), and 0.15 GeV (2.43 GeV/c^2). Quantum-chromodynamics bag-model calculations also predicted a rich spectrum of dibaryons.[21–23] Alternate explanations for spin-dependent data in terms of inelasticities due to the opening of pion production channels, rather than in terms of dibaryon resonances, have been proposed.[15,18,19,24,25] In any case, no theory or phase-shift analysis has successfully accounted for all of the structure in $\Delta\sigma_T$.

We present here the results of two $\Delta\sigma_T$ experiments. The first was performed at the Argonne National Laboratory Zero Gradient Synchrotron (ZGS). It covered the momentum range 1.23–2.48 GeV/c. A conventional transmission technique with scintillation detectors was used for the measurement. The second was performed at the Los Alamos Clinton P. Anderson Meson Physics Fa-

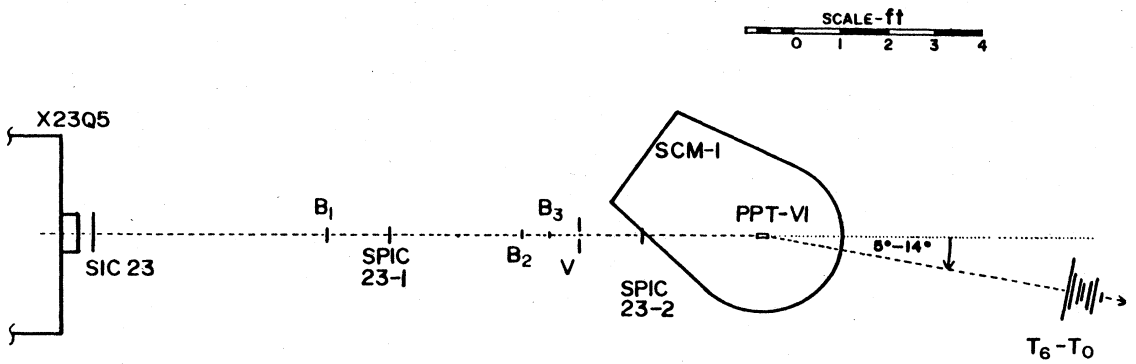

FIG. 1. Plan view of experimental layout at ZGS. PPT-VI, Rice/Argonne polarized proton target. SCM-1, superconducting 2.5-T solenoid. B_1—B_3, beam-defining scintillators. V, veto scintillator. SPIC 23-1 and 23-2, segmented proportional integrating counters. T_1—T_6, transmission scintillation counters. T_0, beam normalization counter.

cility (LAMPF) covering the momentum range 0.81—1.45 GeV/c. This experiment used the same polarized-target cryostat, but employed high-precision ionization chambers for the transmission measurement.

II. EXPERIMENTAL PROCEDURES AND DATA ANALYSIS

A. The polarized proton target

Although different target materials were used at the ZGS and LAMPF, the target assembly and cryogenic equipment were the same (the Rice/ANL polarized proton target PPT-VI). The polarized proton target was a teflon-lined, copper, cylindrical resonant microwave cavity with internal dimensions 2.30-cm diameter×6.99-cm long, positioned in a 25-kG magnetic field and cooled to 0.5 °K by a ^{3}He-^{4}He evaporation cryostat. The cavity was filled with 1-mm-diameter spheres of frozen target material. A NMR coil with an internal diameter of 1.9 cm in the target cavity monitored the polarization of the target material.[26] The NMR system was calibrated using the pure thermal-equilibrium value of the polarization as given by

$$P=\tanh(\mu H/kT)\ ,$$

where μ=proton magnetic moment, H=external magnetic field, k=Boltzmann's constant, and T=temperature of target material. A 70-GHz microwave signal polarized the free-hydrogen protons in the target material by dynamic nuclear polarization. A superconducting magnet (ANL, SCM-1) provided the 25-kG magnetic field with a uniformity of one part in 5000 over a radius of 5 cm.

B. ZGS experimental equipment

The target material used at the ZGS was ethylene glycol [$C_2H_4(OH)_2$] doped with Cr^V paramagnetic centers through a reaction with potassium dichromate ($K_2Cr_2O_7$).[27] The target polarization throughout the experiment was typically 80%.

The ZGS measurements were performed with scintillation detectors arranged as shown in Fig. 1. The detector sizes and their distances from the target are tabulated in Table I. Counters T_0—T_6 were mounted on a platform pivoted about a point directly below the target to facilitate the centering of the transmission detectors for each new beam momentum since the beam was deflected by the transverse magnetic field of the SCM.

The incident beam of 10^5 protons/spill was defined by the coincidence $B=B_1\cdot B_2\cdot B_3\cdot\bar{V}$. The V detector, with a 1.59-cm hole, vetoed the beam halo. A valid event in transmission detector T_6 was defined by the coincidence $B\cdot T_6$. T_6 subtends a larger solid angle than the other detectors so a good event in any of the other detectors must also register in T_6. A valid event in any of the other transmission detectors was defined by $B\cdot T_6\cdot T_i$. The T_0 detector, subtending the smallest solid angle of any of the detectors, was used to monitor the efficiencies of the transmission detectors. The efficiency of transmission detector i is

$$\mathscr{E}_i=\frac{B\cdot T_0\cdot T_i}{B\cdot T_0}\ .$$

Detector efficiencies were >99% throughout the experiment. The accidental rate was measured by having the coincidence timing between B and T_6 offset by 70 nsec

TABLE I. Detector sizes and distances from the target at ZGS.

Detector	Dimensions (cm)[a]	Distance from target (cm)
B_1	7.62×12.7×0.318	279.08
SPIC 23-1	7.62×7.62	240.0
B_2	3.81×0.318	156.85
B_3	2.54×0.318	132.72
V	21.59×10.16×0.635 with 1.59-cm-diam. hole in center	116.84
SPIC 23-2	7.62×7.62	76.2
T_6	40.64×0.635	198.76
T_4	22.86×0.635	202.88
T_2	15.24×0.635	204.47
T_1	10.16×0.635	207.80
T_3	20.32×1.27	214.63
T_5	25.4 ×1.27	216.22
T_0	5.08×0.635	220.66

[a]Horizontal×vertical×thickness or diameter×thickness.

(the ZGS microstructure period). The accidental rate was always $<2\%$.

C. ZGS procedure

For each beam momentum, the transport system was tuned to center a 10-mm-diameter spot on the target. The position of the beam was monitored by two segmented proportional integrating chambers (SPIC 23-1 and SPIC 23-2). The centroid and width of the beam at these two positions was recorded for each beam spill.[28] The proper positioning of all the detectors was checked with Polaroid film at each incident beam momentum.

The beam polarization was reversed on alternate spills. The details of the beam polarimeter calibration are given in Ref. 29. The average beam polarization for the experiment was typically 72%. The data were taken in sets of three to six runs, each lasting twenty minutes. The direction of the target polarization was reversed after each set of runs.

D. ZGS data analysis

Cuts were applied to the singles rate of scintillator B_1 to accept only spills with more than several thousand counts, serving to veto a spill if the beam intensity was low or nonexistent. The B coincidence had similar cuts to reject a spill if the beam happened to be grossly mis-steered. Cuts were applied to the scaler count ratio V/B, which would reject a spill if the beam were moderately mis-steered or if the beam properties had changed. The horizontal and vertical positions of the beam centroid had cuts set to allow a movement of ± 1.5 mm. Cuts on the horizontal and vertical beam widths were treated similarly. Typical fluctuations in the beam position were observed to be $\pm\frac{1}{2}$ mm for an entire run. The maximum difference between the beam "up" and beam "down" average position centroids for an entire run was 0.08 mm.

The value of $\Delta\sigma_T$ for each transmission detector i was calculated from the accumulated scaler counts for each run:

$$\Delta\sigma_{Ti}=\frac{1}{N_0\rho t P_B P_T}\ln\left[(G_i^+/B^+)/(G_i^-/B^-)\right],$$

where $G_i^{\pm}$ = valid events in counter i for target and beam for polarizations parallel (antiparallel). $B^{(\pm)}$ is the accumulated number of protons incident on the target, P_B is the average beam polarization, P_T is the average target polarization, N_0 is Avogadro's number, ρ = density of free protons in the target, 0.073 ± 0.005 g/cm^3, and t is the target thickness 6.99 cm. A weighted average was made of all runs of each beam polarity, resulting in a value of $\Delta\sigma_T$ for up and down target polarization for each detector. A simple average for the up and down values was then calculated for each solid angle, so that

$$\Delta\sigma_{Ti}=\frac{\Delta\sigma_{Ti}^{\uparrow}+\Delta\sigma_{Ti}^{\downarrow}}{2},$$

for each detector.

This procedure cancels any false asymmetries due to misalignment of the transmission counters, or due to deuterons, pions, or inelastically scattered protons, which have bending angles in the PPT magnet different from the transmitted beam. Misalignment of the transmission counters can lead to false asymmetries because of the nonzero analyzing power of p-nucleus scattering, which, even at the small angles observed here, is not negligible

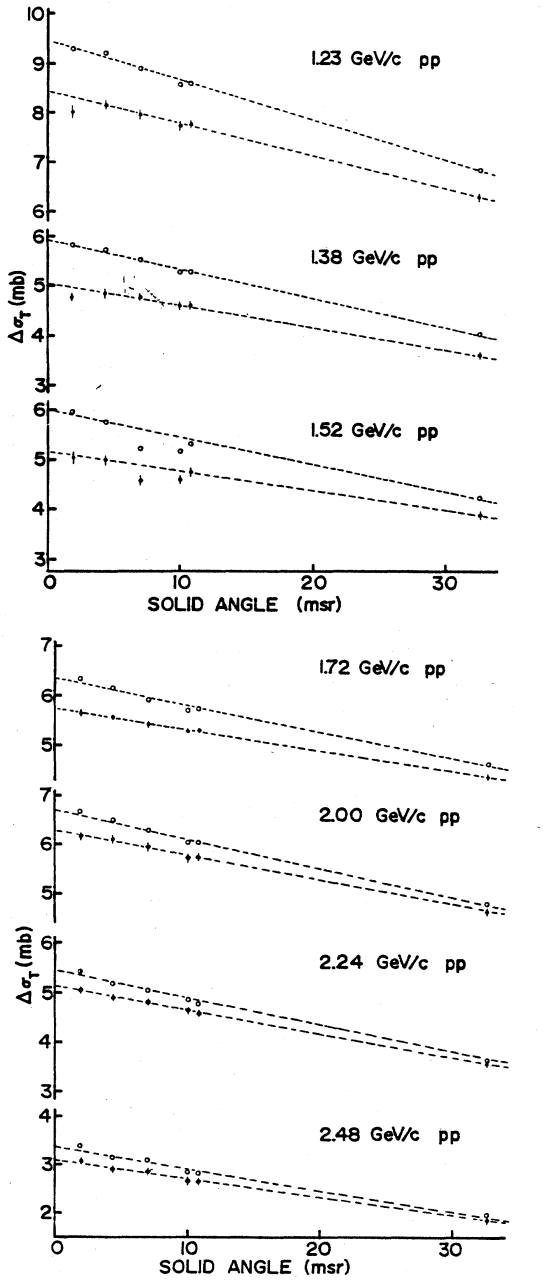

FIG. 2. ZGS data for extrapolation of $\Delta\sigma_T$ to zero solid angle. Open circles (closed circles), with (without) Coulomb-nuclear interference corrections.

compared to the small asymmetry ($\sim 10^{-4}$) from $\Delta\sigma_T$. Provided $P_T^+ \approx P_T^-$, such false asymmetries will cancel in the above average.

The Coulomb-nuclear interference corrections as described by Watanabe[30] were applied to each $\Delta\sigma_{Ti}$, and a linear extrapolation to zero solid angle was made (Fig. 2). The values of $\Delta\sigma_T$ thus derived and the magnitudes of the Coulomb-nuclear interference corrections are tabulated in Table II along with a detailed account of the statistical and systematic errors. Further details of the experiment and data analysis are given in Ref. 31.

E. ZGS errors

The error in the target polarization measurement is 7%, based on a 3% error in measuring the target temperature, a 5% error in determining the area of the thermal-equilibrium NMR curve, and a conservative estimate of a 4% error in the dispersion correction. The error in the beam polarization is 6%.[29] The uncertainty in the density of free protons in the target is 7%. There is a 2% uncertainty in the quoted beam momenta.

F. LAMPF experimental equipment

Two types of target material were used at LAMPF: 1,2 propanediol ($C_3H_8O_2$) prepared with potassium dichromate and 1,2 propanediol mixed with a highly stable and soluble Cr^V complex prepared from sodium dichromate ($Na_2Cr_2O_7$) and 2-ethyl-2-hydroxybutyric acid [$(C_2H_5)_2C(OH)COOH$].[27] The dose delivered to the target during a typical transmission measurement ($\sim 10^{13}$ protons/cm^2) resulted in a reduced polarizability in the beam-target interaction region. The NMR signal was proportional to the average polarization of the entire target sample. It was thus necessary to recalibrate the NMR readout so that it gave a measure of the polarization in the depleted beam-target interaction region. Measurements of the proton-proton elastic-scattering spin-correlation parameter A_{nn} at 90° c.m. were made preceding and following each transmission measurement. The target polarization is then calculated using the values of A_{nn} calculated from Arndt's phase-shift-solution data set FA83 (Ref. 32) (Table II). A two-arm magnetic spectrometer was used to detect the elastically scattered forward and recoil protons in coincidence, discriminating against background quasielastic scatterings.[33] The target polarization is given by

$$P_T = \frac{1}{P_B A_{nn}} \frac{N(\uparrow\uparrow)-N(\downarrow\uparrow)+N(\downarrow\downarrow)-N(\uparrow\downarrow)}{N(\uparrow\uparrow)+N(\downarrow\uparrow)+N(\downarrow\downarrow)+N(\uparrow\downarrow)} ,$$

where $N(ij)$ is the normalized event rate for elastic scattering for beam polarization i and target polarization j, and P_B is the magnitude of the beam polarization (typically 80%).

TABLE II. Summary of results from LAMPF experiment 504 and ZGS experiment 460, measurements of the total-cross-section difference ($\Delta\sigma$) for protons in pure transverse-spin states. The energies quoted are the laboratory beam energies at the center of the target. The $\Delta\sigma$'s are final values, corrected for Coulomb-nuclear interference. The total error is the analysis error determined by a regression analysis and extrapolation to zero solid angle, added in quadrature with the systematic errors in the target polarization, beam polarization, and the 7% error in the target constant (the reciprocal of the product of the target density and target length). The Coulomb-nuclear interference corrections are tabulated under the heading CNI corr. Additional systematic errors are discussed in the text. A_{nn} values are from Arndt's phase-shift-analysis data set FA83 (Ref. 32).

Energy (MeV)	Momentum (GeV/c)	$\Delta\sigma_T$ (mb)	Errors					CNI corr (mb)	A_{nn} (90°)
			Total (mb)	Analysis (mb)	Target pol (mb)	$(N_0\rho t)^{-1}$ (mb)	Beam pol (mb)		
304	0.81	−1.59	1.02	0.55	0.83	0.23	0.04	1.73	0.700[b]
436	1.00	5.75	0.75	0.28	0.61	0.33	0.09	1.20	0.502
485	1.07	8.61	1.00	0.21	0.82	0.51	0.15	1.10	0.467
519	1.12	8.48	1.24	0.20	1.10	0.52	0.15	1.21	0.480
536	1.14	10.37	0.99	0.19	0.69	0.65	0.19	1.16	0.495
571	1.18	12.22	1.52	0.21	1.27	0.79	0.23	1.01	0.538
587	1.20	10.04	1.32	0.53	1.02	0.63	0.18	0.89	0.560
620	1.24	7.84	0.60	0.04	0.31	0.49	0.14	0.86	0.603
637	1.27	7.26	1.10	0.13	0.99	0.45	0.13	0.75	0.622
689	1.33	6.05	0.69	0.07	0.57	0.37	0.11	0.78	0.665
741	1.39	5.64	0.39	0.07	0.13	0.35	0.10	0.72	0.683
791	1.45	5.92	1.09	0.13	1.02	0.37	0.10	0.69	0.683
609[a]	1.23	9.44	0.93	0.06	0.56	0.56	0.48	1.27	
730[a]	1.38	5.92	0.55	0.04	0.33	0.33	0.29	1.06	
848[a]	1.52	5.97	0.59	0.07	0.35	0.35	0.30	0.90	
1021[a]	1.72	6.33	0.65	0.03	0.39	0.39	0.34	0.71	
1271[a]	2.00	6.70	0.72	0.05	0.43	0.43	0.37	0.49	
1490[a]	2.24	5.44	0.59	0.04	0.35	0.35	0.30	0.37	
1713[a]	2.48	3.36	0.36	0.04	0.22	0.22	0.19	0.31	

[a]Indicates data from ZGS experiment E-460.
[b]80°.

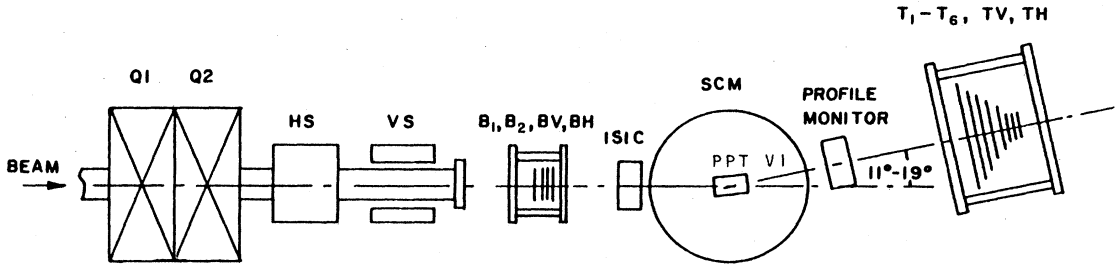

FIG. 3. Plan view of experimental layout at LAMPF. PPT-VI, Rice/Argonne polarized proton target. SCM-1, superconducting 2.5-T solenoid. B_1 and B_2, beam ionization chambers. *BV*, *BH*, *TV*, and *TH*, split ionization chambers. T_1-T_6, transmission ionization chambers. ISIC and PM, profile monitors. *HS* and *VS*, steering magnets. $Q1$ and $Q2$, quadrupole doublet.

In some cases the target polarizability was degraded by as much as 30%. The calibration factor, relating the NMR signal to the target polarization seen by the beam, was derated linearly with dose from the value determined by elastic scattering preceding the transmission measurements to that following. The target polarization for a particular run was given by the average NMR measurement for that run multiplied by the derated calibration factor. Target polarizations ranged from 50% to 75%.

The LAMPF measurements, like the ZGS measurements, were standard good geometry attenuation experiments. The experimental arrangement is shown in Fig. 3. The detector sizes and their distances from the target are tabulated in Table III.

Ionization chambers were used in the LAMPF experiment to take advantage of the low duty factor (3—6%), high-current beam. A typical average beam current was 10^9 protons/sec. With 40 spills/sec, the instantaneous rate during the 750-μsec spill was 3×10^{10} protons/sec.

The beam chamber, measuring the incident beam, contained two 12.7-cm-diameter parallel-plate ionization detectors, one with a gap of 0.953 cm and the other with a gap of 0.635 cm. The two sizes made it possible to correct for electron-ion recombination in the detectors, an effect which is proportional to the length of the detector gap to first order. The transmission chamber contained six parallel-plate ionization detectors with diameters of 12.7 to 30.5 cm, and all with gap lengths of 0.635 cm. Both chambers were filled with pure argon to a pressure of 760 mm Hg absolute. An amplifier and 14-bit analog-to-digital converter (ADC) were connected to each detector. The beam spills were 750-μsec duration with a repetition rate of 40 Hz (120 Hz at 689 and 741 MeV). The collector electrodes were all grounded until the start of a beam spill. After a delay at the end of the spill, all of the ADC's were simultaneously strobed. Midway between successive beam spills an identical routine was followed to provide a background measurement. The beam polarity was reversed once per minute. During the ten seconds required for the reversal, a precisely determined charge was applied to the collectors with a 16-bit digital-to-analog converter (DAC) to check the stability of the electronics.

The line B polarimeter LBPO, situated in the beam line 14 m upstream of the experimental cave, measured the beam polarization, typically $\geq 80\%$, with an accuracy of $\pm 2\%$.[34] The LBPO measured the left-right asymmetry in the elastic scattering at 17° of the protons from a thin CH_2 target. The quasielastic background was rejected by requiring a coincidence between the forward arms at 17° and their respective conjugate arms at 66°.

The vertical and horizontal centroids of the incident and transmitted beams were measured with a precision of 10^{-4} cm with split-plate ionization detectors in the beam and transmission chambers. The beam position and size were also monitored with a precision of 1 mm with the beam-profile monitors PM1 and PM2 positioned immediately upstream and downstream of the target.

G. LAMPF procedure

For each beam momentum the transport system was tuned to provide a 6—10-mm-diameter spot centered on the target. Fine adjustments to the focusing and position were made with quadrupole magnets $Q1$ and $Q2$ and steering magnets *VS* and *HS*. The beam spot size and position with respect to the target cavity were checked by the double exposure of a Polaroid film. For the first exposure, the beam was defocused with $Q1$ and $Q2$, giving an outline of the target cavity and NMR coil. For the

TABLE III. Detector sizes and distances from the target at LAMPF.

Detector	Dimensions (cm)[a]	Distance from target (cm)
HS	Horizontal steering magnet	320
VS	Vertical steering magnet	290
B_1	12.7 ×1.91	130.0
B_2	12.7 ×1.27	127.8
BV	12.7 ×1.27	126.5
BH	12.7 ×1.27	125.2
ISIC	7.62×7.62×1.27	76
PM	7.62×7.62×2.54	38
T_6	30.48×1.27	130.0
T_5	27.62×1.27	128.7
T_4	24.77×1.27	127.4
T_3	21.59×1.27	126.2
T_2	17.78×1.27	124.9
T_1	12.7×1.27	123.6
TV	12.7 ×1.27	122.4
TH	12.7 ×1.27	121.1

[a]Horizontal×vertical×thickness or diameter×thickness.

second exposure, the beam was properly focused, giving an image of the spot superimposed on the image of the cavity.

The calibration constant relating the polarization of the target in the region intersected by the beam to the NMR signal was measured with elastic scattering runs, each of 40-min duration, for both target polarities. The transmission measurements were taken in sets of four 20-min runs. The beam polarity was reversed every minute. The target polarity was reversed after each set of runs. This procedure was continued for a total of three target polarity reversals. After the transmission measurements, the NMR calibration constant was again measured by elastic scattering.

H. LAMPF data analysis

There were large systematic dependences of $\Delta\sigma_T$ produced by electron-ion recombination and the position-dependent response of the chambers. The position dependence of the chamber responses was caused by nonparallel collector and high-voltage electrodes. The gap separation from one edge of a detector to the other typically varied by 0.005—0.012 cm, which, on the 12.7-cm-diameter detector, was sufficient to give a gain variation of 0.08% for a spot displacement of 0.25 cm. Since $\Delta\sigma_T$ is calculated from the ratio of the transmissions, a gain variation of this magnitude from one beam polarization state to the other would be equivalent to a cross-section difference of 4 mb. A multiple regression was performed to remove the dependence of $\Delta\sigma_T$ on changes in beam current, electron-ion recombination, and beam spot position from one beam polarization state to the other.

Since the beam polarity was reversed once per minute, the shortest period for which the cross-section difference can be calculated is two minutes. For the purpose of the multiple regression, a data point was defined as the cross-section difference formed by averaging the transmission over a 1-min period, during which the beam polarity was constant, and calculating its ratio to the average transmission for the following 1-min period of constant beam polarity. Calculating $\Delta\sigma_T$ from the data in this way resulted in 60—80 values of $\Delta\sigma_T$ for each of the six solid angles, target polarity, and energy. The systematic dependence of $\Delta\sigma_T$ for a given target polarity was modeled by the equation (for the ith transmission detector and the kth value of $\Delta\sigma_T$)

$$\Delta\sigma_{ik}=\Delta\sigma_{Ti0}+A_{1i}\Delta B_{2k}+A_{2i}\Delta\left[\frac{B_1}{B_2}\right]_k$$

$$+A_{3i}\Delta T_{Vk}+A_{4i}\Delta T_{Hk}\ .$$

Here $\Delta\sigma_{ik}$ is the value of $\Delta\sigma_T$ for detector i calculated from the kth pair of 1-min-intervals measurements. The regression was carried out over the four experimentally measured variables $\Delta B_{2k},\Delta(B_1/B_2)_k,\Delta T_{Vk},\Delta T_{Hk}$, to determine the coefficients $A_{1i},A_{2i},A_{3i},A_{4i}$. $\Delta\sigma_{Ti0}$ is the constant that is determined by this regression.

ΔB_{2k} is the deviation from the average beam current as measured by beam-chamber detector 2 (0.635-cm gap), for the kth pair of 1-min intervals. This variable is included to remove systematic effects dependent on a change in the beam current from one beam polarity to the other.

$\Delta(B_1/B_2)_k$ is the deviation from the ratio of the average beam current measured by B_1 to that measured by B_2. This variable is included to remove the effect of a difference in recombination from one beam burst to the next.

ΔT_{Vk} is the deviation from the average values of the vertical position of the beam centroid. This variable removes the effect of the change in detector response due to a vertical beam spot displacement.

ΔT_{Hk} is the deviation from the average values of the horizontal position of the beam centroid. This variable removes the effect of the change in detector response due to a horizontal beam spot displacement.

Figure 4 shows histograms of typical 2-min data points versus $\Delta\sigma_T$ values for the first transmission counter before and after the regression analysis. The value before regression is $\Delta\sigma_{1k}$, the raw experimental value. The value after regression is the reduced $\Delta\sigma_T$ given by

$$\Delta\sigma'_{1k}=\Delta\sigma_{1k}-\left[A_{11}\Delta B_{2k}+A_{21}\Delta\left[\frac{B_2}{B_2}\right]_k+A_{31}\Delta T_{Vk}\right.$$

$$\left.+A_{41}\Delta T_{Hk}\right]\ .$$

The centroid of $\Delta\sigma'_{ik}$ is the constant $\Delta\sigma_{Ti0}$ determined by the regression. As can be seen in Fig. 4, the regression analysis substantially reduces the spread in the values of $\Delta\sigma_T$. There is, however, an offset between the data with target spin up and spin down. As discussed in Sec. II D, these false asymmetries may be reduced by averaging the target spin-up (+) and spin-down (−) values of $\Delta\sigma_{Ti0}$ for each detector to give the value

$$\Delta\sigma_{Ti}=w^+\Delta\sigma^+_{Ti0}+w^-\Delta\sigma^-_{Ti0}$$

for the ith solid angle. Here $w^\pm$ is the weight calculated from the statistical errors in $\Delta\sigma^\pm_{Ti0}$, as determined from the regression analysis. This target-spin-averaged value was not changed by the regression analysis within the errors given in Table II.

The Coulomb-nuclear interference correction was applied at each of the six solid angles,[30] and a linear extrapolation to zero solid angle was then made. The extrapolations are shown in Fig. 5. A linear extrapolation gave a poor fit to the 304-Mev $\Delta\sigma_{Ti0}$ data. This is because the angular distribution for the reaction $pp\rightarrow\pi d$ has a cusp within the solid angle of the chambers. Therefore, the 304-MeV data set was truncated to the first three ioniza-

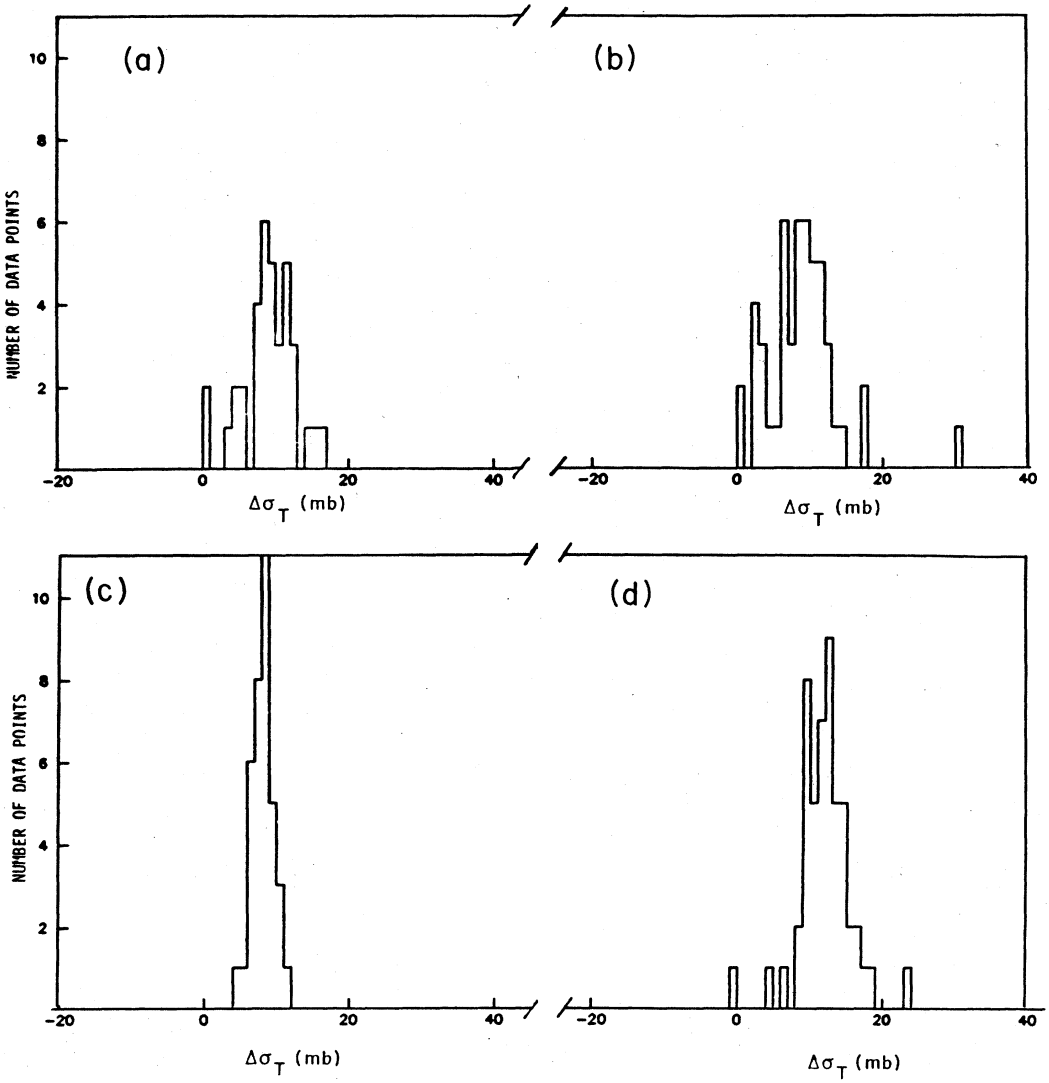

FIG. 4. Histogram of the number of data points versus $\Delta\sigma_T$ values for the first transmission detector at 571 MeV. The data before the regression analysis are shown for target polarization (a) up and (b) down, and after regression analysis for target polarization (c) up and (d) down. Each $\Delta\sigma_T$ value is calculated from the transmission data averaged over a 1-min period of beam polarity up, followed by a 1-min period of beam polarity down.

tion chambers. The $pp \rightarrow \pi d$ cusp lies outside the solid angle subtended by the chambers (and the scintillators for the ZGS measurement), at all other energies. The values of $\Delta\sigma_T$ and a detailed account of the errors are given in Table II.

I. LAMPF errors

The total error, listed in Table II, is the error determined by the regression and extrapolation to zero solid angle added in quadrature with the systematic errors in the target polarization, beam polarization, and target constant $(N_0\rho t)^{-1}$. The target-polarization error results from the statistical error in the elastic-scattering data, the systematic error of 2% in the beam polarization, and the error in the NMR measurement. The error of 7% in the target constant results from the uncertainty of the target length and the free-proton density. The error of 2% in the beam polarization was estimated from quench-ratio measurements at LAMPF.[34] The Coulomb-nuclear interference correction in the last column of Table I is the amount by which $\Delta\sigma_T$ is increased by the correction. Further details of the experiment and data analysis are given in Ref. 32.

III. CONCLUSIONS

Figure 6 compares the present data with the TRIUMF (Stanley *et al.*[8]) and LAMPF (Ditzler *et al.*[9]) results, and our previous ZGS data (Biegert *et al.*[7]). The two Rice ZGS measurements were made with scintillators and the

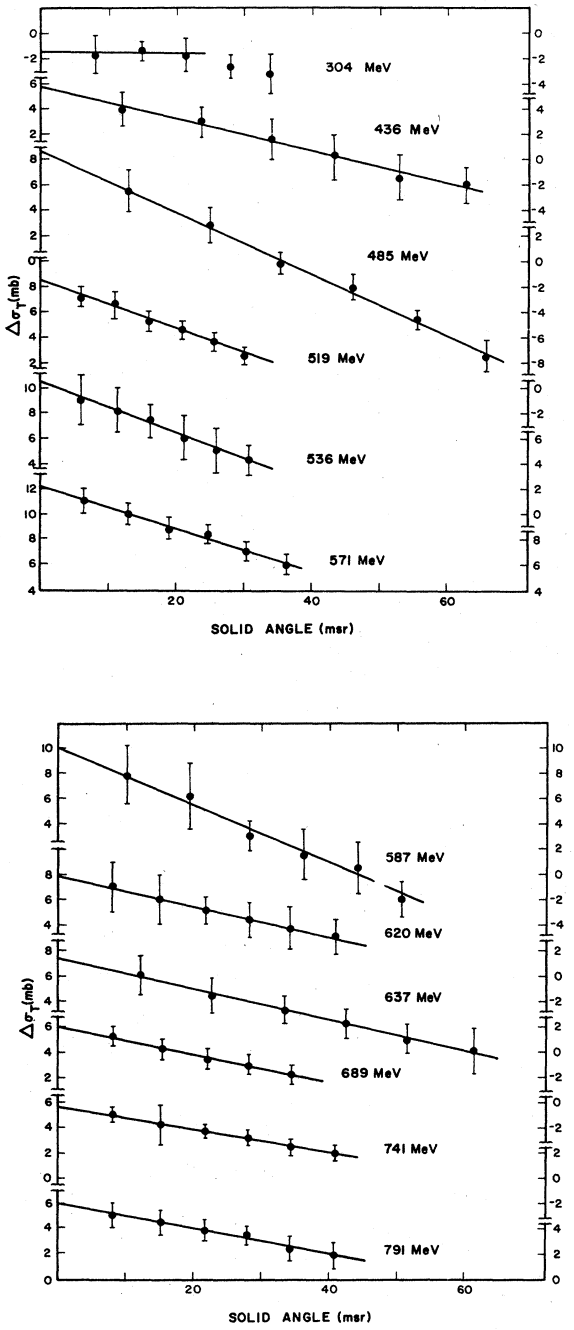

FIG. 5. LAMPF data for extrapolation of $\Delta\sigma_T$ to zero solid angle. Data have been corrected by the regression analysis, averaged over target polarizations and corrected for Coulomb-nuclear interference effects.

Rice LAMPF measurements were made with ionization chambers. These two different techniques required completely different detector response corrections. However, these experiments did share the same PPT and NMR systems. The TRIUMF group used scintillators and a target similar to the Rice PPT. The data taken at LAMPF by the Argonne group were taken with scintillators and a frozen-spin target. The errors shown on all the data sets are statistical only. Stanley *et al.* quote a 6.9% systematic error, and Biegert *et al.* estimate a 12% systematic error. The total errors, systematic and statistical added in quadrature, are given in Table II for both of the present data sets. These errors range from 0.4 to 1.5 mb. The corresponding total error ranges for Stanley *et al.* are 0.4—1.1 mb; for Ditzler *et al.*, 0.5—0.6 mb; and for Biegert *et al.*, 0.5—1.2 mb.

The current Rice-ZGS and Rice-LAMPF data are in excellent agreement. The peak near $\sqrt{s}=2.14$ GeV shown in Fig. 5 is well established, appearing in both the TRIUMF and present data. The two experiments agree on the magnitude of the peak (10—12 mb), although the Rice data reaches the 10-mb level at a beam kinetic energy about 40 MeV higher than the TRIUMF data. Our higher-momentum ZGS data and the earlier ZGS data show a broad structure centered at $\sqrt{s}=2.43$ GeV. The lowest two energies of the earlier ZGS data lie significantly below the present data. Finally, the data of Ditzler *et al.* lie significantly lower than the TRIUMF data and the present data. The reason for this discrepancy is not known. However, one should notice that although there is some normalization discrepancy among the various sets of data, the shape of the $\Delta\sigma_T$ versus energy is consistent. The measurement of $\Delta\sigma_T$ is a challenging experimental problem. To achieve an accuracy of 0.5 mb, one must determine the ratio of transmissions for beam and target spins antiparallel to beam and target spins parallel to an accuracy of $1:10^4$. Therefore, considering the precision required in the determination of the transmission ratios and the potential for error in the measurements of the beam and target polarizations, the agreement among the five sets of data is rather good.

The values of $\Delta\sigma_T$ calculated from Arndt's phase-shift-analysis program[33] using the data base SP84 are shown as the solid curve in Fig. 5. The values calculated from the Dubois *et al.*[37] phase-shift set are shown as the dashed curve. All previously published $\Delta\sigma_T$ data[7–9] are in the SP84 data base. The Ditzler *et al.* data are not included in the Dubois *et al.* data base. The present data are not included in either set. The Arndt curve has a centroid agreeing with that of the data, but the shape and magnitude differ from the data. The Dubois *et al.* curve has a peak about the right magnitude, but it occurs at a higher momentum.

The narrow peak at 1.18 GeV/c ($m=2.14$ GeV/c^2) and broad structure at 2.0 GeV/c ($m=2.43$ GeV/c^2) correspond to the masses of the proposed dibaryon resonances $^1D_2$ and $^1G_4$, respectively.[12,20] The Argand plots for the $^1D_2$ phase shifts for both solutions show looping behavior which could be interpreted as an inelastic dibaryon resonance. However, this interpretation is not unique and the behavior can also be attributed to strong inelastic-threshold effects. Grein and Kroll[38] have performed scattering-amplitude analysis of forward nucleon-nucleon scattering using dispersion relations. They do not find a $^1D_2$ resonance and only weak evidence for a $^1G_4$ ($m=2.39$ GeV/c^2) resonance. To clarify the situation the

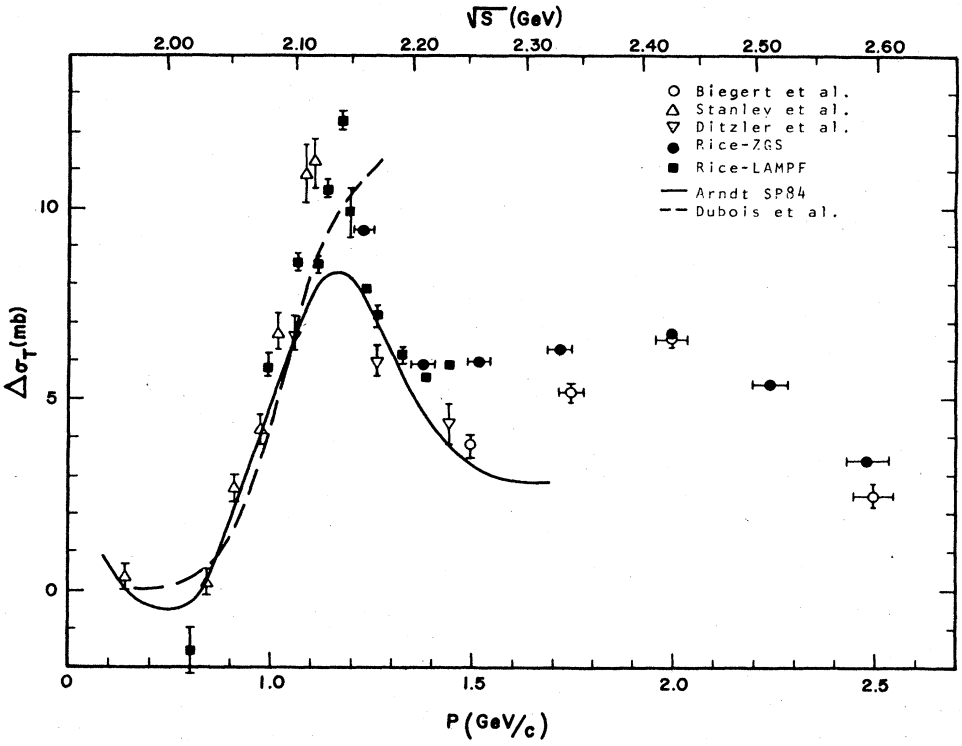

FIG. 6. $\Delta\sigma_T$ versus incident momentum. The errors shown are statistical only. The errors are dominated by systematic effects, see Table II. Previous experimental results of Biegert *et al.* (Ref. 7), Stanley *et al.* (Ref. 8), and Ditzler *et al.* (Ref. 9) are shown. The solid curve is the prediction of Arndt's phase-shift solution SP84 (Ref. 33). The dashed curve is calculated from the phase-shift solution of Dubois *et al.* (Ref. 37). The data of Biegert *et al.* have been reanalyzed to include Coulomb-nuclear interference corrections (Ref. 35). The lowest-energy point (not shown) near 1.20 GeV/c is unreliable (Ref. 36).

discrepancy in the elastic data[39] must be resolved and more spin-dependent inelastic data is needed.

ACKNOWLEDGMENTS

We gratefully acknowledge the cooperation and expertise extended to this experiment by the entire staff of LAMPF, particularly Olin Van Dyke, Michael McNaughton, Robert Macek, and Richard Werbeck. This work was supported by the U.S. Department of Energy.

*Present address: NL Industries, Houston, TX.
†Present address: Shell Development Company, Houston, TX.
‡Present address: Exxon Production Research Corp., Houston, TX.
§Present address: Physics Dept., U.S. Naval Academy, Annapolis, MD.
**Present address: Getty Oil Corp., Houston, TX.
††Present address: C Division, Los Alamos National Laboratory, Los Alamos, NM.
‡‡Present address: CERN, Geneva, Switzerland.
§§Present address: State University of New York at Stony Brook, Stony Brook, NY.

[1]M. Jacob and G. C. Wick, Ann. Phys. (N.Y.) **7**, 404 (1959).
[2]M. L. Goldberger *et al.*, Phys. Rev. **120**, 2250 (1960).
[3]E. F. Parker *et al.*, Phys. Rev. Lett. **31**, 783 (1973).
[4]W. deBoer *et al.*, Phys. Rev. Lett. **34**, 558 (1975).
[5]G. L. Kane and G. H. Thomas, Phys. Rev. D **13**, 11 (1976); **13**, 2944 (1976).
[6]D. W. Joynson, J. Phys. G **2**, L65 (1976).
[7]Ed. K. Biegert *et al.*, Phys. lett. **73B**, 235 (1978).
[8]J. P. Stanley *et al.*, Nucl. Phys. **A403**, 525 (1983).
[9]W. R. Ditzler *et al.*, Phys. Rev. D **22**, 680 (1983).
[10]M. Arik and P. G. Williams, Nucl. Phys. **B136**, 425 (1978).
[11]R. Bandari, *et al.*, Phys. Rev. Lett. **46**, 1111 (1981).
[12]N. Hoshizaki, Prog. Theor. Phys. **57**, 1099 (1977); **58**, 716 (1977); **60**, 1796 (1978); and **61**, 129 (1979).
[13]K. Hidaka *et al.*, Phys. lett. **70B**, 479 (1977).
[14]T. Ueda, Phys. Lett. **74B**, 123 (1978).
[15]C. L. Hollas, Phys. Rev. Lett. **44**, 18 (1980); **44**, 1186 (1980).
[16]P. J. Mulders, Phys. Rev. D **25**, 5 (1982); **25**, 1269 (1982).
[17]Bonnie J. Edwards, Phys. Rev. D **23**, 9 (1981); **23**, 1978 (1981).
[18]W. M. Kloet and R. R. Silbar, Phys. Rev. Lett. **45**, 970 (1977);

Nucl. Phys. **A338**, 291 (1980); **A338**, 317 (1980).
[19]W. M. Kloet, J. A. Tjon, and R. R. Silbar, Phys. Lett. **99B**, 80 (1981).
[24]J. A. Niskanen, Phys. Lett. **122B**, 17 (1982).
[25]J. Arvieux, Phys. Lett. **103B**, 99 (1981).
[26]J. A. Buchanan and J. M. Clement, IEEE Nucl. Sci. **26**, 4014 (1979).
[27]R. C. Fernow, in *High Energy Physics with Polarized Beams and Polarized Targets,* proceedings of the Third International Symposium, Argonne, Illinois, 1978, edited by G. H. Thomas (AIP, New York, 1978), p. 15 and references therein.
[28]F. Greeley *et al.*, IEEE Nucl. Sci. **16**, 891 (1969).
[29]H. Spinka *et al.*, Nucl. Instrum. Methods **24**, 239 (1983).
[30]Y. Watanabe, Phys. Rev. D **19**, 1022 (1979).
[31]J. D. Lesikar, Ph.D. thesis, Rice University, 1981.
[32]W. P. Madigan, Ph.D. thesis, Rice University, 1984.
[33]R. A. Arndt, SAID (scattering analysis interaction dial-in) computing facility, Virginia Polytechnic Institute and State University.
[34]M. W. McNaughton, Phys. Rev. C **23**, 1128 (1981).
[35]J. D. Lesikar, M. A. thesis, Rice University, 1980.
[36]At 1.2 GeV/c depolarization in the ZGS caused systematic errors in the measurement of the beam polarization [see Spinka *et al.* (Ref. 29)].
[37]R. Dubois *et al.*, Nucl. Phys. **A377**, 554 (1982).
[38]W. Grein and P. Kroll, Nucl. Phys. **A377**, 505 (1982).
[39]J. Bystricky *et al.*, contribution to the Ninth International Conference on High Energy Physics and Nuclear Structure, Versailles, 1981 (unpublished). The Saclay group has unpublished $\Delta\sigma_T$ data from 0.99 to 3.2 GeV/c. Preliminary values of these data have been included in the phase-shift analyses and amplitude analysis.
[20]A. Yokosawa, Phys. Rep. **64**, 2 (1980); **64**, 50 (1980).
[21]R. L. Jaffe, Phys. Rev. Lett. **38**, 195 (1977); **38**, 612 (1977).
[22]P. J. Mulders *et al.*, Phys. Rev. Lett. **40**, 1543 (1978).
[23]P. J. Mulders, A. T. Aerts, and J. J. de Swart, Phys. Rev. D **21**, 2653 (1980).